NASA TECHNICAL MEMORANDUM NASA TM-88486

STUDY BY DOUBLE EXPOSURE HOLOGRAPHY OF THE THREE-DIMENSIONAL CHARACTER OF THE FLOW AROUND AN AIRFOIL PROFILE IN A WIND TUNNEL

G. Heid and M. Stanislas

Translation of "Etude par holographi à double exposition du caractere tridimensionnel de l'écoulement autour d'un profil d'aile en soufflière", Institut de Mécanique des Fluides de Lille, Lille, France, Report No. 80/31, July 3, 1980, pp. 1-34 (82N22474).

NATIONAL AERONAUTICS AND SPACE ADMINISTRATION
WASHINGTON, D.C. SEPTEMBER 1986

Table of Contents

List of Symbols

l : chord of the profile

$2B$: span of the jet stream

x, y, z : coordinates in the object space

x', y', z' : coordinates in the image space

u, v, w : component of the velocity

ζ : complex variable : $\zeta = y + iz$

U_0 : velocity at distance

I : aerodynamic incidence

α : geometric incidence

α_i : induced incidence

c_z : coefficient of aerodynamic lift

δ^* : thickness of displacement of the boundary layer

δ : thickness of the boundary layer

μ : vortical intensity

D_p : diameter of a particle

ν : kinematic viscosity of the fluid

ρ : voluminal mass of the fluid

ρ_p : voluminal mass of the particles

μ : viscosity of the fluid

The notations of section 3.1.1 are are peculiar to it.

STUDY BY DOUBLE EXPOSURE HOLOGRAPHY OF THE THREE-DIMENSIONAL CHARACTER OF THE FLOW AROUND AN AIRFOIL PROFILE IN A WIND TUNNEL

G. Heid and M. Stanislas

Institute of Fluid Mechanics of Lille, France

1. Objective of the Study /1*

The objective of the study is to demonstrate the tridimensional character of the flow around a profile placed between walls and to evaluate the incidence induced with the assistance of measurements of velocities by double exposure holography, in order to be able to compare with the values obtained by the theory of Menard.

2. Description of the Experimental Assembly

2.1 Model

The profile utilized is a NACA 0012 profile, of chord 1 = 80 mm, equipped with 36 pressure pick-ups. The table of the coordinates of these pressure pick-ups is presented in figure 1.

2.2 Wind Tunnel

Figure 2 presents a diagram of the principle of the assembly utilized.

The wind tunnel functions by aspiration and includes:

-a zone with constant cross-section of 390 x 700 with 200 m length, including a rim of ϕ 100 mm at the intake, and a honeycomb at the outlet;

*Numbers in the margin indicate pagination in the foreign text.

-a convergent of length of 600 mm and a contraction ratio of 19;

-an experimental jet stream of length of 780 mm, height of 350 mm and width of 42 mm. The walls of this jet stream are aluminum plates including a glass porthole of interferometric quality designed to allow the passage of the laser beam for recording. One of the portholes is pierced in order to be able to attach the model and to make the tubes of the pressure pick-ups exit;

-a diffuser of length of 1 m and of ratio of 3.3;

-a centrifuge ventilator of 0.6 m diameter, whose flow can be adjusted.

Figure 3 presents a photo of the wind tunnel.

2.3 Means of Measurement

In order to accomplish an exploration of the boundary layer, a stop-bolt of 0.5 mm diameter has been manufactured. This thus has allowed obtainment of measurements of stopping pressure at a distance of 3/10 of a mm from the wall.

This bolt is mounted on a micrometer allowing obtainment of the displacements in 1/100 of a mm. This micrometer is inserted into a special plate also including static pressure orifices of ϕ 2/10 of a mm (figure 4). This allows the obtainment of the longitudinal and transversal distributions of static pressure. /2

The photo of figure 3 demonstrates the bolt in place in the jet stream.

2.4 Holographic Sequence

2.4.1 Principle and Description

The principle of the method is recalled (figure 6). A transpar-

ent object, which in this case a a mist of micro-drops, is illuminated by a coherent light beam. If the mist is not too dense, a portion of the beam traverses it without being deflected and forms the reference beam. Each particle intercepts a portion of the light and diffuses it into an object beam. Due to their coherence, the two beams interfere on a photographic plate which has been placed behind the object.

Once the plate is developed, if it is exposed to a beam identical to the reference beam, there can be observed the tridimensional image of the initial object. In order to have more details on the method, the reader is referred to reference [1].

The sequence that has been accomplished has been described in detail in reference [2]. It includes two parts:

-a sequence of recording which includes a two impulse ruby laser (figure 7) and an orientable hologram support. This sequence carries out the recording of two successive holograms on the same photographic plate with a specific interval of time;

-a sequence of restitution which allows the reconstitution and observation of the image after development of the plate. It is composed of a helium-neon laser, a piloted hologram-carrier plate and a closed circuit television (figure 8).

2.4.2 Method of Analysis

Figure 9 presents the convention that has been selected for the reference trihedrons. In the recording, the usual trihedron is utilized in order to describe the flow on the profile. In the restitution, the trihedron is defined by the direction of displacement of the tables.

The sequence of restitution allows obtainment of the three coordinates (x', y', z') of the image of a droplet with respect to the image of an origin engraved on the lateral walls, in order to determine /3

the coordinates x, y, z of the drop with respect to this same origin in the object-space, there are applied the formulae for the holography [reference 3]. However, in order to determine these coordinates with precision, the following factors must be taken into account:

-the two lasers do not have the same wavelength, which influences the magnification of the image;

-for convenience of assembly and in order to limit the aberrations due to the optical pieces, the recording and the restitution are carried out in slightly divergent light, which also modifies the magnification;

-finally, in the restitution, the hologram is deplaced with respect to the axis of the beam, which deforms the image.

By taking into account these factors, it has been possible to discover the coordinates of different references (cross hairs, micrometric sights) with a precision on the order of 0.5% on the transversal variations Δx and Δy.

Taking into account the precision on Δt, there can be estimated at 1.5% the precision on the components according to Ox and Oy of the velocity of the particles. This precision could be improved by the utilization of a counter in order to measure Δt. On the contrary, taking into account the fact that the flow is quasi bidimensional, Δz is small, and the precision along Oz is much worse.

In order to process the data relative to the analysis, there has been implemented a program on a computer. The data from the digital displays are entered in raw form on a perofrated tape. The program carries out the transformations and the changes of references necessary, then outputs the results in printed and graphed form.

2.4.3 Seeding

The velocimeter by double exposure holography is an optical meth-

od which necessitates the seeding of the flow. This is carried out with the assistance of the mocro-droplets of water generated by a Napier type atomizer. A jet of water fed by a capillary tube is fractured by a concentric jet of compressed air whose generating pressure can be adjusted (figure 10).

The density of the mist can thus be adjusted and the distribution of diameter centered on the value desired (recall that the diameter of the particles is distributed according to a law of Weibull) [reference 4].

The atomizer is placed upstream of the collector in a fashion such that the particles have the time to become adapted to the velocity of the flow.

The particles of a diameter of 10 to 20 μm have been retained for /4 the measurements of velocities.

3. The Theory of Menard

It is very difficult to accomplish the infinite elongation in wind tunnels because the transversal distribution of the velocities between two parallel walls of a jet stream is not bidimensional. Boundary layers are developed along these walls and thus induce notable divergences between the results obtained in different wind tunnels for the same profile.

A method for correction of the effects of lateral boundary layers in incompressible fluid has been proposed by M. Menard [5].

3.1 Theoretical Questions

3.1.1 The Theory of Thin Profiles

A thin profile is considered in a perfect isovolume air flow, extending to infinity where the velocity is uniform and designated U_0.

The flow is permanent and irrotational. The reference conventions are carried by figure 11. There is designated as α the incidence, as u and v the velocities of perturbation and as ϕ the potential of the velocities. It is assumed that u and v are very small compared to U_0 and that $\cos \alpha \simeq 1$, $\sin \alpha \simeq \alpha$, the profile being thin and the incidence small.

The equations are thus linearized and allow processing of the problem by the fundamental solution of the following system:

$$\begin{cases} \dfrac{\partial^2 \phi}{\partial x^2} + \dfrac{\partial^2 \phi}{\partial y^2} = 0 \\ \dfrac{\partial \phi}{\partial y} = U_0 (h'(x) - \alpha) \text{ for } y = 0 \text{ and } |x| \leq \frac{1}{2} \\ \text{grad } \phi \longrightarrow 0 \text{ at infinity.} \end{cases}$$

The method is valid at small incidences and it is imprecise at the leading edge, u and v then not being negligible compared to U_0.

The profile being symmetrical, the flow then can be considered as the superimposition of the flow around this profile without incidence and the flow around a level plate in incidence.

The first problem is processed by taking a linear distribution of sources on the chord of the profile and leads to the following solution: /5

$$u = \frac{U_0}{\pi} \int_{-l/2}^{+l/2} h_E(\xi) \frac{(x-\xi)^2 - y^2}{\left[(x-\xi)^2 + y^2\right]^2} d\xi$$

and

$$v = \frac{2U_0 y}{\pi} \int_{-l/2}^{+l/2} h_E(\xi) \frac{(x-\xi)}{\left[(x-\xi)^2 + y^2\right]^2} d\xi$$

h_E designating the ordinate of the upper surface.

The second problem is processed by taking a linear distribution of vortices on the chord of the profile and leads to the following solution:

$$u = \frac{\alpha U_0}{\pi} \int_{-l/2}^{+l/2} \sqrt{\frac{l/2 - \xi}{l/2 + \xi}} \; \frac{y}{(x-\xi)^2 + y^2} \, d\xi$$

and

$$v = \frac{-\alpha U_0}{\pi} \int_{-l/2}^{+l/2} \sqrt{\frac{l/2 - \xi}{l/2 + \xi}} \; \frac{x-\xi}{(x-\xi)^2 + y^2} \, d\xi$$

A calculation program formulated from this method allows obtainment of the modulus and the direction of the velocity at any point of the plane.

3.1.2 The Theory of Prandtl

The flow is considered around an airfoil of finite but great extension. The airfoil and its wake are replaced by the standard vortical system (figure 12).

The free vortices are detached on the edge of the flight. The vortical intensity on a thin strip of material of width dy is equal to the variation at this point of the circulation along the airfoil line:

$$\mu_y = \frac{\partial \mu}{\partial y} \, dy.$$

The velocity induced at point M, situated at a distance y_1 from the median section, by a thin strip of material of intensity μ_y escaping from the edge of the flight of the airfoil at the distance y from the median section has for a component on Oz:

$$dw = -\frac{1}{2} \cdot \frac{1}{2\pi} \frac{r_y}{(y - y_1)} = -\frac{1}{4\pi} \cdot \frac{\partial r}{\partial y} \cdot \frac{dy}{(y - y_1)}$$

From this:

$$w = -\frac{1}{} \int^{+B} \frac{\partial \Gamma}{} \cdot \frac{dy}{}$$

If the flow is compared around the profile to that which would exist in plane movement, one is led to introduce the notion of induced incidence: this is the ratio of the velocity w on the line relating to U_0. /6

3.2 The Systems for Replacement of the Finite Span Airfoil

Menard depends on the following experimental observations:

-presence of two marginal vortices in the wake of the airfoil;

-the marginal vortices do not possess the properties of the vortices in perfect fluid unless the viscosity is taken into account.

3.2.1 Equivalent Vortical Diagram

The real airfoil is replaced by a lifting surface constituted of vortical thin strips of material arranged parallel to the span of the airfoil. These vortices are connected to the airfoil and their circulation is considered as constant the length of the span.

In a given section, the airfoil profile is replaced by its framework; the vortical elements constituting the attached vortices must be distributed on this line, conforming to the theory of thin profiles.

At the ends of the airfoil, the elementary vortices are juxtaposed in order to give birth to two marginal vortices of circulation μ_0 downstream from the edge of the flight. A simplification consists of replacing the connected vortices by a single vortex placed in the focus of the profiles. Under these conditions, the origin of the two marginal vortices is in the focus. This is the scheme known under the name of "horseshoe system".

a) Determination of the Circulation of the Marginal Vortices

With the preceding approximation, there is obtained, conforming to the theorem of Joukowski:

$$\Gamma_0 = c_{z_\beta} u_0 \frac{l}{2} = I\left(dC_{z\infty}/dI\right) u_0 \frac{l}{2}$$

where I is the aerodynamic incidence of the profile and $dC_{z\infty}/dI$ is the slope of the unitary curve of lift of the profile for the experimental infinite extension.

Thus the determination of the circulation of the marginal vortices is carried out by making an abstraction of the velocities which they induce on the airfoil.

b) Calculation of the Velocities Induced at One Point of a Finite Span Airfoil

The velocity induced in perfect fluid at a point A by a vortex element of length OM and of circulation μ_0 is given by the formula of Biot and Savart (figure 13):

$$w = \frac{\Gamma_0}{} \int^{\theta_0} \frac{d\theta}{}$$

Since $\rho = r/\cos\theta$, w is then expressed by: /7

$$w = \frac{\Gamma_0}{4\pi r} \int_0^{\theta_0} \cos\theta \, d\theta = \frac{\Gamma_0}{4\pi r} \sin\theta_0$$

In figure 14 there are represented a rectangular airfoil and two marginal vortices $\pm\mu_0$ escaping from the airfoil at points M1 and M2 such that $M_0M_1 = M_0'M_2 = l/4$ on abscissa of the focus.

The velocities induced along Oz by the vortices 1 and 2 at the point A are respectively:

$$w_1 = \frac{\Gamma_0}{4\pi(B-y)} \int_{\theta_1}^{\pi/2} \cos\theta \, d\theta = \frac{\Gamma_0}{4\pi(B-y)} (1 - \sin\theta_1)$$

and

$$w_2 = \frac{\Gamma_0}{4\pi(B+y)} (1 - \sin\theta_2)$$

The resultant induced velocity at A is equal to:

$$w = w_1 + w_2 = \frac{\Gamma_0}{4\pi} \left\{ \left(\frac{1 - \sin\theta_1}{B-y} \right) + \left(\frac{1 - \sin\theta_2}{B+y} \right) \right\}$$

In particular, for the median section, there is obtained:

$$w(y=0) = \frac{\Gamma_0}{4B} (1 - \sin\theta_0)$$

3.2.2 Utilization of the System for Replacment for the Study of the Influence of the Lateral Boundary Layers on the Tests Between Panels

The conditions on the lateral walls are satisfied by the image vortices. The equivalent vortical system is represented in figure 15. Menard proposes to arrange the marginal vortices at a distance from the walls equal to the thickness of displacement of the lateral boundary layer.

The complex potential for the file of vortices + μ_0, from step 2B and ordinates ±a is thus written, with a = B - δ^* and ζ = y + iz:

$$F_1(\zeta) = -i\frac{\Gamma_0}{2\pi} \left\{ \operatorname{Log}(a+\zeta) + \sum_1^\infty \operatorname{Log}\left[(a+\zeta)^2 + 4m^2B^2 \right] \right\}$$

Also for the file $-\mu_0$:

$$F_2(\zeta) = i\frac{\Gamma_0}{2\pi} \left\{ \operatorname{Log}(\zeta-a) + \sum_1^\infty \operatorname{Log}\left[(\zeta-a)^2 - 4m^2B^2 \right] \right\}$$

For the two files, the complex potential is: /8

$$F(\zeta) = \frac{i\Gamma_0}{2\pi}\left\{\log\frac{(\zeta+y)\left[(\zeta+y)^2+4B^2\right]\left[(\zeta+y^2)+3B^2\right][\cdots][(\zeta+y)^2+4m^2B^2]}{(\zeta-y)\left[(\zeta-y)^2-4B^2\right]\left[(\zeta-y^2)-3B^2\right][\cdots][(\zeta-y)^2-4m^2B^2]}\right\}$$

By developing, there is obtained the formula of Villat:

$$F(\zeta) = -\frac{i\Gamma_0}{2\pi}\log\frac{\sin\frac{\pi(\zeta+a)}{2B}}{\sin\frac{\pi(\zeta-a)}{2B}}$$

The free vortices derived from the airfoil in fact are only semi-infinite and the preceding expression must be divided by 2. The complex velocity is thus written:

$$\frac{dF}{d\zeta} = i\frac{\Gamma_0}{4B}\cdot\frac{\sin\frac{\pi a}{B}}{\cos\frac{\pi a}{B}-\cos\frac{\pi\zeta}{B}} \qquad (1)$$

At a point of the plane z = 0, the vertical component of the velocity is:

$$w = \frac{\Gamma_0}{4B}\cdot\frac{\sin\frac{\pi a}{B}}{\cos\frac{\pi a}{B}-\cos\frac{\pi y}{B}}$$

In particular, for the median section, there is:

$$w(y=0) = \frac{\Gamma_0}{4B}\cdot\frac{\sin\frac{\pi a}{B}}{\cos\frac{\pi a}{B}-1} = \frac{\Gamma_0}{4B}\cdot\frac{\sin\frac{\pi(B-\delta^*)}{B}}{\cos\frac{\pi(B-\delta^*)}{B}-1}$$

Menard defines two fictitious vortices situated at P and P', ends of the airfoil, and thus the circulation μ_0' is defined such that the value of w at A (focus of the profile of the median section) induced by these vortices are identical to that induced at the same point by the vortices $\pm\mu_0$ and their images (figure 16).

$$w_A = \frac{2\Gamma_0'}{4\pi B} = \frac{\Gamma_0'}{2\pi B} = \frac{\Gamma_0}{4B} \quad \frac{\sin\frac{\pi(B-\delta^*)}{B}}{\cos\frac{\pi(B-\delta^*)}{B} - 1}$$

The airfoil between panels can then be replaced by an airfoil of finite span 2B and the velocity induced by the marginal vortices of circulation $\pm\mu_0'$ can be calculated at all points of the median section.

In particular, the velocity induced at point A' is equal to:

$$w_A' = \frac{\Gamma_0'}{2\pi B}(1 - \sin\theta_0)$$

By replacing μ_0' by its value, there results:

$$w_A' = \frac{\Gamma_0}{4B} \quad \frac{\sin\frac{\pi(B-\delta^*)}{B}}{\cos\frac{\pi(B-\delta^*)}{B} - 1} (1 - \sin\theta_0)$$

There can then be calculated the angle induced at all points of the median section of an airfoil placed between panels: /9

$$\alpha_i(y=0) = \frac{\Gamma_0}{4B U_0}\left[\frac{\sin\frac{\pi(B-\delta^*)}{B}}{\cos\frac{\pi(B-\delta^*)}{B} - 1}\right](1 - \sin\theta_0)$$

$$\alpha_i(y=0) = -\frac{\Gamma_0}{4B U_0} \operatorname{tg}\frac{\pi\delta^*}{2B}(1 - \sin\theta_0)$$

In particular, there is obtained the overall incidence induced at the focus of the airfoil for $\theta_0 = 0$:

$$\alpha_i(x=0, y=0) = -\frac{\Gamma_0}{4B U_0} \operatorname{tg}\frac{\pi\delta^*}{2B}$$

3.2.3 Simplified Vortical Diagram

The replacement of the two files of vortices $\pm\mu_0$ constituting the

the equivalent system proposed by Menard by two fictitious vortices constitutes a limitation to the validity of the previously presented formula. In fact, this relationship does not allow calculation of the incidence induced at any points of space other than a point of the axis Ox. The authors have sought to estimate the incidence induced at all points by replacing the model by a lifting segment placed at the focus and extended toward downstream by two vortices in perfect fluid situated at the distance δ^* from the lateral walls.

The method of the images is applied in order to take into account stresses exerted on the fluid by the walls, while being limited to the first four images:

$$F_1(\zeta) = -i\frac{\Gamma_1}{2\pi}\log\left(\zeta-(B-\delta^*)\right)$$
$$F_2(\zeta) = +i\frac{\Gamma_2}{2\pi}\log\left(\zeta+(B-\delta^*)\right)$$
$$F_3(\zeta) = +i\frac{\Gamma_2}{2\pi}\log\left(\zeta-(B+\delta^*)\right)$$
$$F_4(\zeta) = -i\frac{\Gamma_2}{2\pi}\log\left(\zeta+(B+\delta^*)\right)$$

The potential of these four vortices is:

$$F(\zeta) = i\frac{\Gamma_1}{2\pi}\log\left[\frac{\zeta-(B+\delta^*)}{\zeta-(B-\delta^*)}\right]+i\frac{\Gamma_2}{2\pi}\log\left[\frac{\zeta+(B-\delta^*)}{\zeta+(B+\delta^*)}\right]$$

$$F(\zeta) = i\frac{\Gamma_1}{2\pi}\log\frac{1-\delta^*/(\zeta-B)}{1+\delta^*/(\zeta-B)}+i\frac{\Gamma_2}{2\pi}\log\frac{1-\delta^*/(\zeta+B)}{1+\delta^*/(\zeta+B)}$$

This expression has been calculated by utilizing the following values: /11

$$c_z = 0.8;\quad \delta^* = 1.5\text{ mm};\quad l = 80\text{ mm};\quad 2B = 42\text{ mm}.$$

The curves of figure 19 demonstrate that α_i decreases very rapidly when it is extended toward upstream. On the contrary, toward downstream, α_i increases and is stabilized at a constant value at the edge of the flight. This value demonstrates in other respects that suffi-

Translators note: page 10 missing

ciently far, everything occurs as if the demi-vortices were infinite. The induced incidence α_i decreases when it is extended from the profile toward the top or toward the bottom.

The curves of figure 20 demonstrate the transversal development of α_i for different abscisses. These curves are voluntarily limited to y = 10 mm, this zone corresponding to the portion of the flow outside of the boundary layer. The development is symmetrical with respect to the median plane of the jet stream.

4. Tests

4.1 Preliminary Tests

These tests have allowed ensurance of the quality of the flow within the jet stream by measuring the intensity of the turbulence and by determining the distribution of static pressure.

The intensity of the turbulence, measured at the hot wire, is 0.33% without atomizer and 0.4% with the atomizer. The measurements of static pressure have not demonstrated any appreciable variation from the upstream toward the downstream over approximately 1 and a half chords and on theother hand from the emplacement of the model. From top to bottom of the jet stream, they indicate, at the abscissa of the leading edge, a relative variation of thevelocity of 0.2%.

4.2 Boundary Layer

An initial transveral summary of pressures has demonstrated that the boundary layer was not turbulent. It has been necessary to preceed with an artificial triggering through the intermediary of a band of sheet glass glued transversally at the output of the collector. The curves of figures 19 and 20 demonstrate that the profiles obtained on the two walls are not completely identical. The thicknesses of the boundary layers obtained are 10.32 mm on the laser side and 11 mm on the hologram side. The thicknesses of displacement are respectively

1.57 and 1.61 mm.

4.3 Results /12

The tests have been carried out at a velocity of 24 m/s. The Reynolds based on the chord of the profile was $1.28\ 10^5$. From an experimental polar obtained rapidly with the assistance of four points, it has been decided to carry out the tests at an incidence close to 8°, which still corresponds to the range of linear variation of Cz (figure 21). It is observed that the experimental Cz is lower than the value $2\pi I$ of the theory of thin profiles.

The effects of high and low walls yields a correction of incidence in degrees which can be estimated at approximately 0.64 Cz. The formula of Menard yields an overall induced incidence $d_i(y = 0)$, taken at the focus of the profile, close to 3.06 Cz in degrees.

For a given aerodynamic incidence, corresponding to an experimental Cz, the curves of figure 21 furnish the overall induced incidence. At constant Cz, this is the difference between the value of the incidence obtained on the experimental polar corrected for the effects of high and low walls and that given by the theoretical courve $2\pi I$. For example, at 8° of aerodynamic incidence, the curves yield 2.7°, against 1.95° by the theory of Menard. This result is satisfactory, but it is necessary not to forget that it does not take into account the viscosity. In fact, the theoretical value $2\pi I$ constitutes an upper boundary for Cz. The fact of taking into account the Reynolds effect reduces the slope of the theoretical polar and thus contributes to reduce the previously cited deviation.

Measurements of velocities by holography were carried out at 30 mm upstream of the leading edge. No systematic variation with span of α_i has been able to be demonstrated in this section (figure 24).

This result is in agreement with the calculation which demonstrates that at this abscissa, the incidence induced is negligible.

In the face of this result, it has been thought to measure the induced incidence itself. For this, it is necessary either to carry out the measurements in a zone perturbed very little by the profile, in a fashion to eliminate the inherent aerodynamic field of the profile, or to know the local inclination of the velocity in plane movement.

The first solution has been discarded because the zones less perturbed by the profile are also those where the influence of the lateral walls is negligible.

The difference between the local incidence measured and the theoretical one, obtained by the theory of thin profiles, yields the value of α_i.

At one point of the flow, the local velocity is the result of three contributions:

-that of the profile; /13

-that of the high and low walls;

-that of the lateral walls.

If it is placed far enough upstream of the profile, the theory of Menard demonstrates that the velocity induced by the lateral walls is negligible.

A calculation demonstrates that at 30 mm upstream from the leading edge, the velocity induced by the high and low walls is also negligible.

Given this, at this point, the velocity of the flow calculated by plane movement and thatmeasured by holography must coincide. Now, in order to obtain this result, it has been necessary for the calculation to adjust the incidence of the profile. There is thus obtained an

aerodynamic incidence of 6.5° corresponding to a Cz measured of 0.58. The theoretical curve $2\pi I$ furnishes a value of 5.5°.

The observed deviation can be attributed at least partially to the Reynolds effect. Nevertheless, it would be necessary to confirm these deviations with other incidences in order to conclude in definitive fashion.

The true value of the aerodynamic incidence of 6.5° determined above has then been utilized for measurements in the vicinity of the leading edge where an induced incidence should exist.

The measurements have been made at 10 mm upstream of the leading edge with particles of mean diameter of 15 μm (figure 23). There is obtained a mean induced incidence of α_i of 4°, a mean calculated with 27 points of measurement, and a standard deviation of 2.33°. The mean value obtained is clearly greater than that of the theory of Menard. The standard deviation reflects a significant dispersion of the results of measurements. This is surprising taking into account the fact that the flow in jet stream vacuum does not present any fluctuation.

It is believed that it isnecessary to investigate the cause of the deviation between the actual local incidence and that furnished by the micro-particles in their inertia. To this end, it has been sought to know the behavior of the water particles subjected to the plane flow produced by the profile.

The simplified equation for themovement of the particle is given by:

$$\frac{d\vec{u}_p}{dt} = \frac{3}{4} C_D \, Re_p \, \frac{\mu}{\rho_p D_p^2} \left(\vec{u} - \vec{u}_p\right)$$

with

$$Re_p = \frac{\rho \, | \vec{u} - \vec{u}_p | \, D_p}{\mu}$$

The drag coefficient is given by a law verified experimentally in uniform flow for Rep $\leq$ 200: /14

$$C_D = \frac{24}{Re_p}\left(1 + 0{,}15\ Re_p^{0{,}687}\right)$$

The calculation consists of sending particles of given diameter upstream of the profile with the velocity of the fluid for initial velocity. This is then repeated over time and the velocity of the particle is calculated by taking for velocity of the fluid that calculated.

This process, applied to micro-droplets of water, of 15 microns and 20 microns diameter, has yielded respectively an angle of 3° and 5° between their trajectories and the current lines, in the zone where the analyses ahve been carried out. This significant deviation reduces rapidly when it is extended from the leading edge.

5. Conclusion

The overall induced incidence, determined with the assistance of the experimental polar, leads to a satisfactory result in comparison with the value furnished by the formula of Menard.

The induced incidence itself has not been measured, but a deviation has been observed by collating the local incidence of the velocity measured in guided jet stream and the theoretical flow around the profile without walls. The local measurements thus furnish values clearly greater than those provided by the vortical theory of Menard. However, taking into account the inertia of the particles and the low value in this zone, there has been little chance to demonstrate a local induced incidence.

It is clear that the problem of the inertia of the micro-particles constitutes the key which allows judgement of the precision of the measurements. It is thus necessary to proceed with a qualifica-

tion of the tracers by calculating their behavior around the profile, in order to determine the zones where the inertia is negligible, and where the induced incidence is measurable.

The determination of α_i must also be refined, by taking into account the boundary layer on the profile in order to calculate the field of velocities in infinite atmosphere.

Finally it is necessary to proceed with analyses downstream of the profile, the effects of the induced incidence being more significant there, thus more easily measurable.

REFERENCES

1. Vienot, J.C., P. Smigielski and H. Royer, Optical holography, development, applications, Dunod, 1971.

2. Dyment, A. and M. Stanislas, "Validation of a velocimetry method by double exposure holography of micro-particles", Report IMFL No. 78/37 on DRET convention no. 77-312.

3. Goodman, J.W., "Introduction to FOURIER optics and holography", Masson and Cie.

4. Haertig, J., "The particles in laser anemometry", Doppler Anemometry with Laser, DISA-LDA Course, March 5-7, 1979.

5. Menard, M., "Contribution to the aerodynamic study of the airfoil and of the helix", PST of the Minister of the Air No. 262, 1950.

6. Dyment, A, Upper aerodynamic course, "Thin airfoil profiles in isovolume fluid".

List of Figures

Figure 1. Table of the sides of the pressure pick-ups.

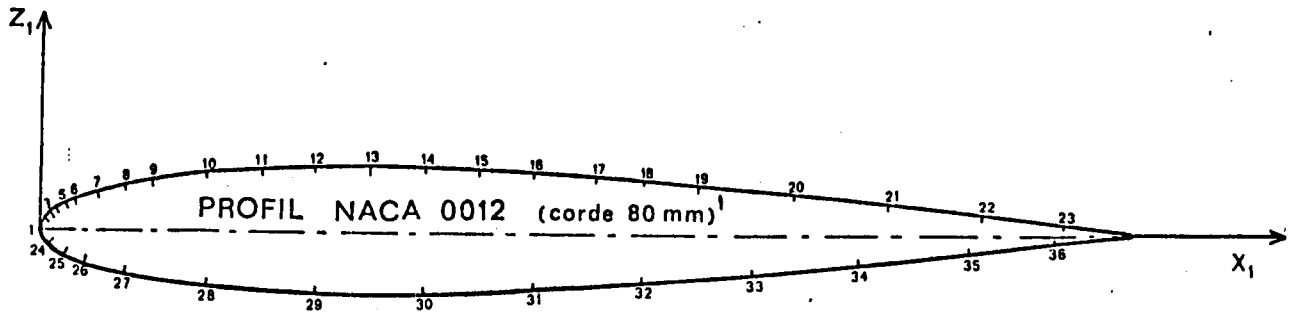

EXTRADOS

Prises de pression	1	2	3	4	5	6	7	8	9	10	11	12	13	14	15	16	17	18	19	20	21	22	23
x_1 mm	0	0.22	0.64	1.02	1.63	2.43	4.05	6.04	8.04	12.04	16.07	20.04	24.07	28.09	32.08	36.08	40.57	44.07	48.08	55.04	62.08	69.08	75.07
z_1 mm	0	0.73	1.225	1.53	1.905	2.285	2.86	3.33	3.75	4.27	4.59	4.76	4.80	4.77	4.65	4.47	4.21	3.96	3.65	3.03	2.31	1.52	0.78

INTRADOS

Prises de pression	24	25	26	27	28	29	30	31	32	33	34	35	36
x_1 mm	0.64	1.65	3.17	5.99	12.02	20.01	28.04	36.05	44.05	52.04	60.07	68.05	75.05
z_1 mm	1.225	1.91	2.58	3.36	4.28	4.76	4.77	4.47	3.95	3.29	2.52	1.64	0.77

Key: 1-NACA 0012 Profile (chord 80 mm) 2-Upper surface 3-Pressure pick-ups 4-Under surface 5-Pressure pick-ups.

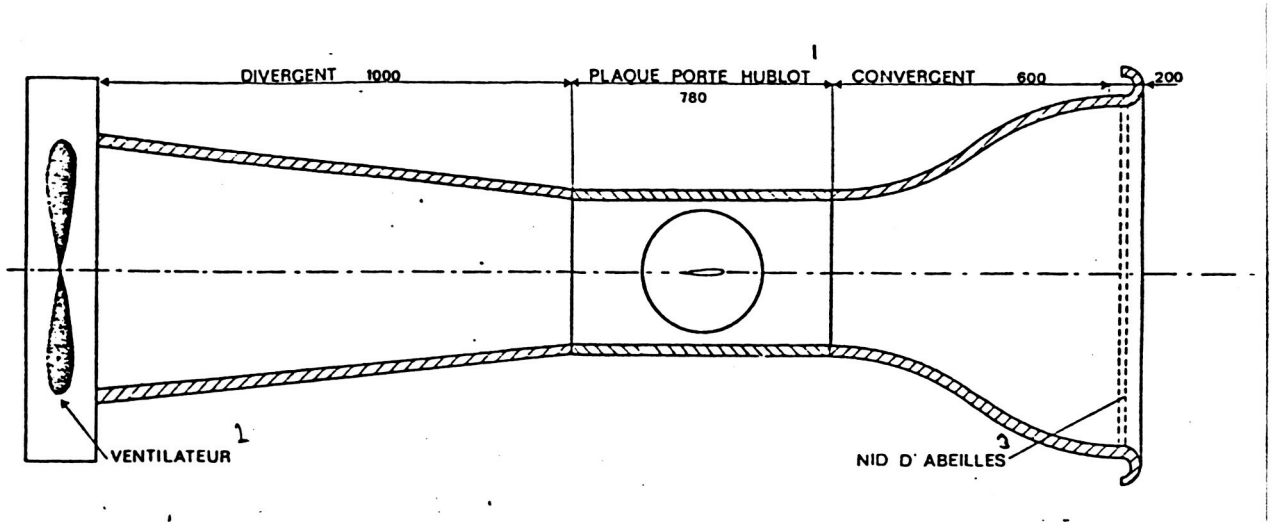

Figure 2. Diagram of principle.

Key: 1-Hublot Carrier plate 2-Ventilator 2-Honeycomb.

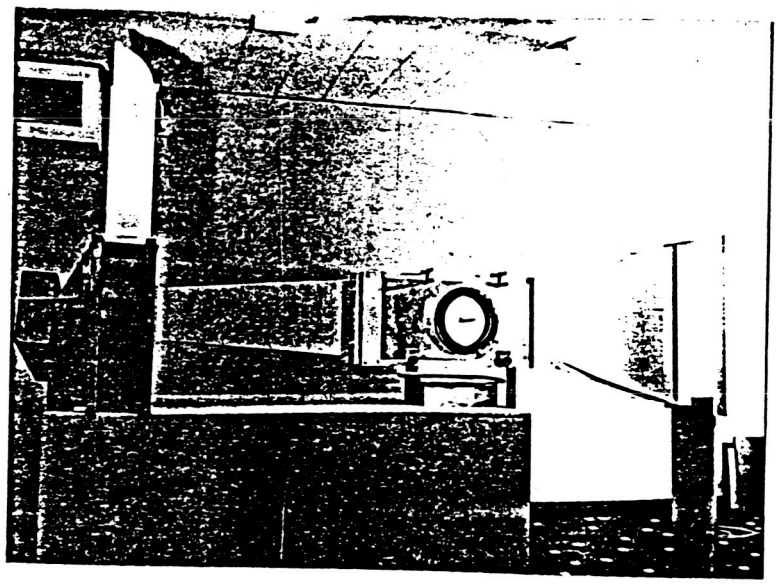

Figure 3. Wind tunnel.

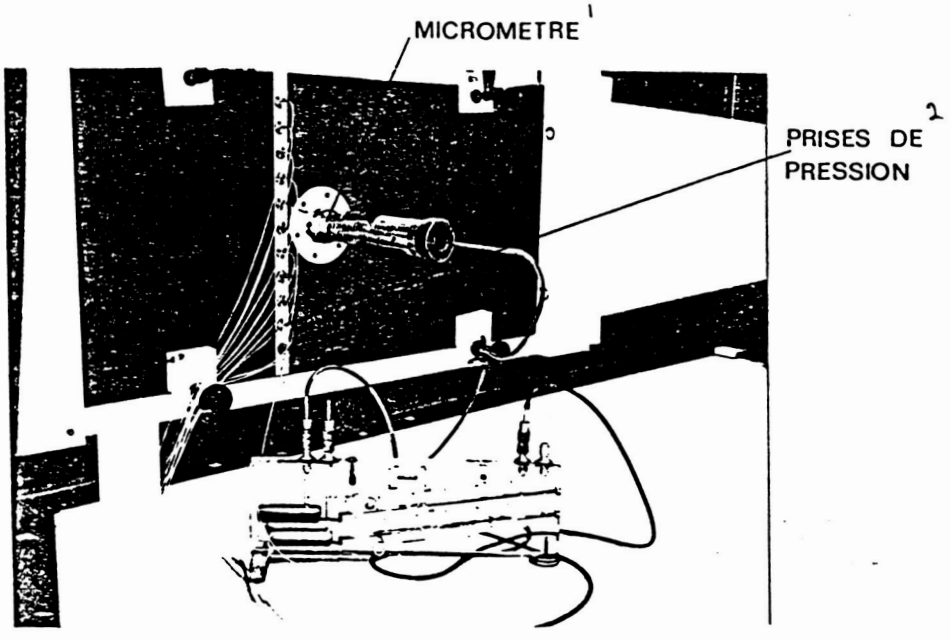

Figure 4. Measurement plate.
Key: 1-Micrometer 2-Pressure pick-ups.

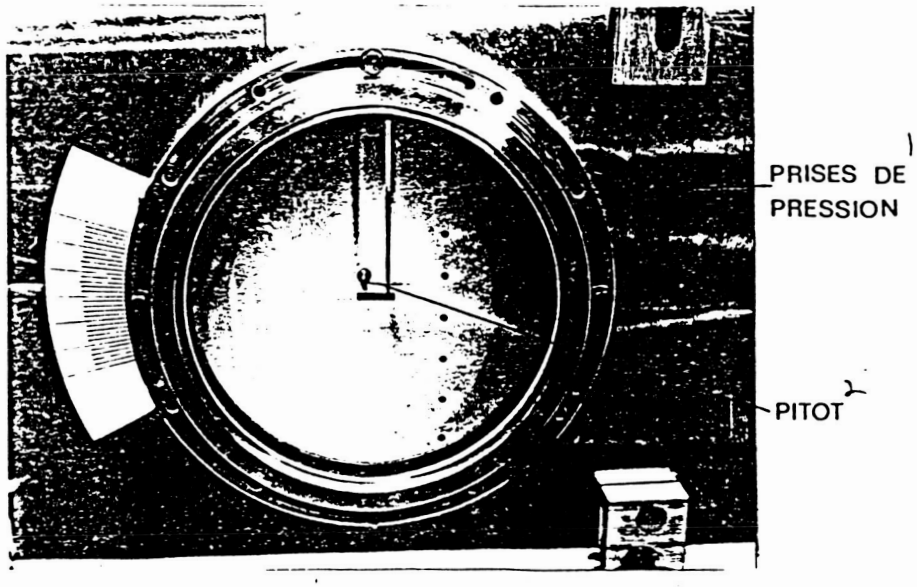

Figure 5. Bolt.
Key: 1-Pressure pick-ups 2-Bolt.

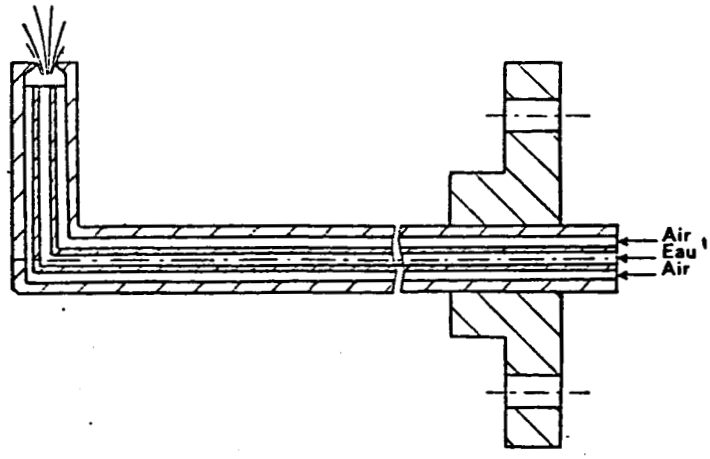

Figure 10. Diagram of principle of the injector.
Key: 1-Water

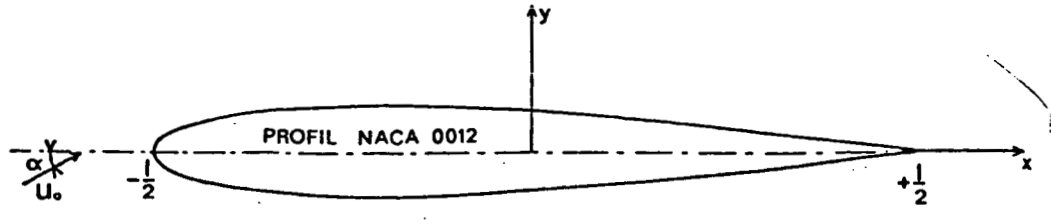

Figure 11. Theory of thin reference profiles.

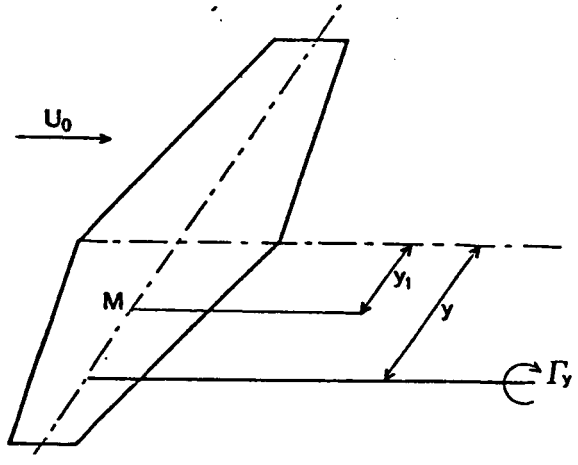

FIGURE 12

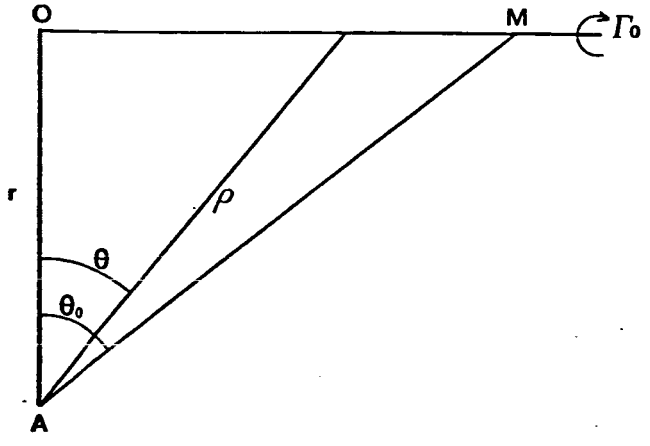

FIGURE 13

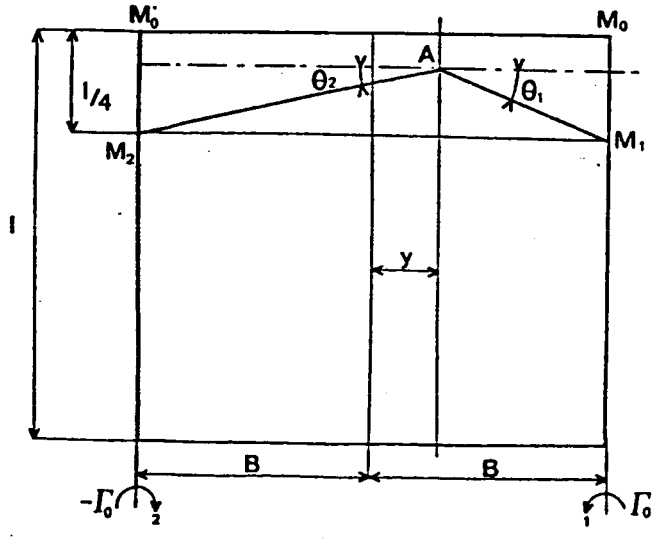

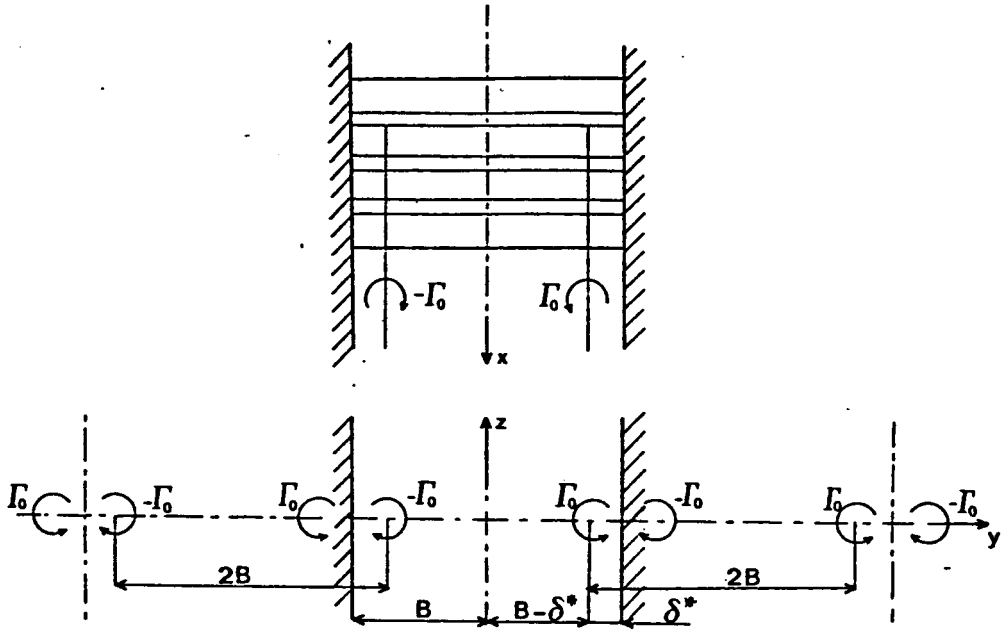

FIGURE 15

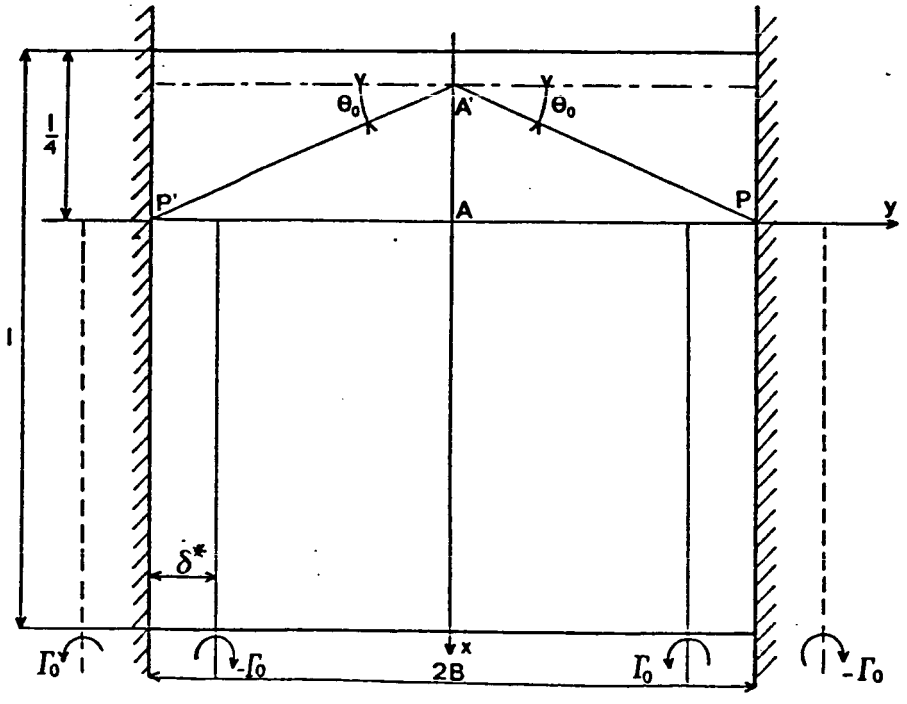

FIGURE 16

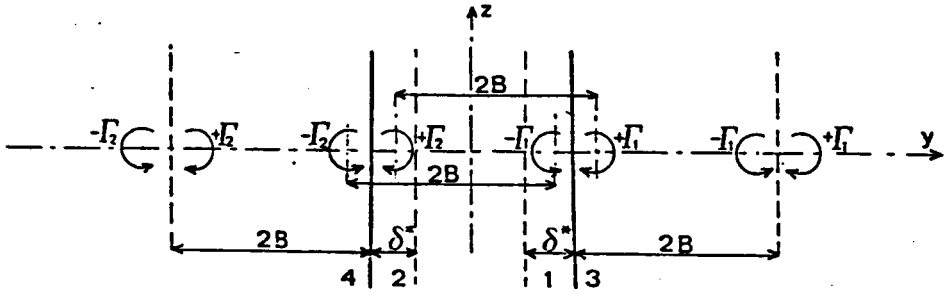

FIGURE 17

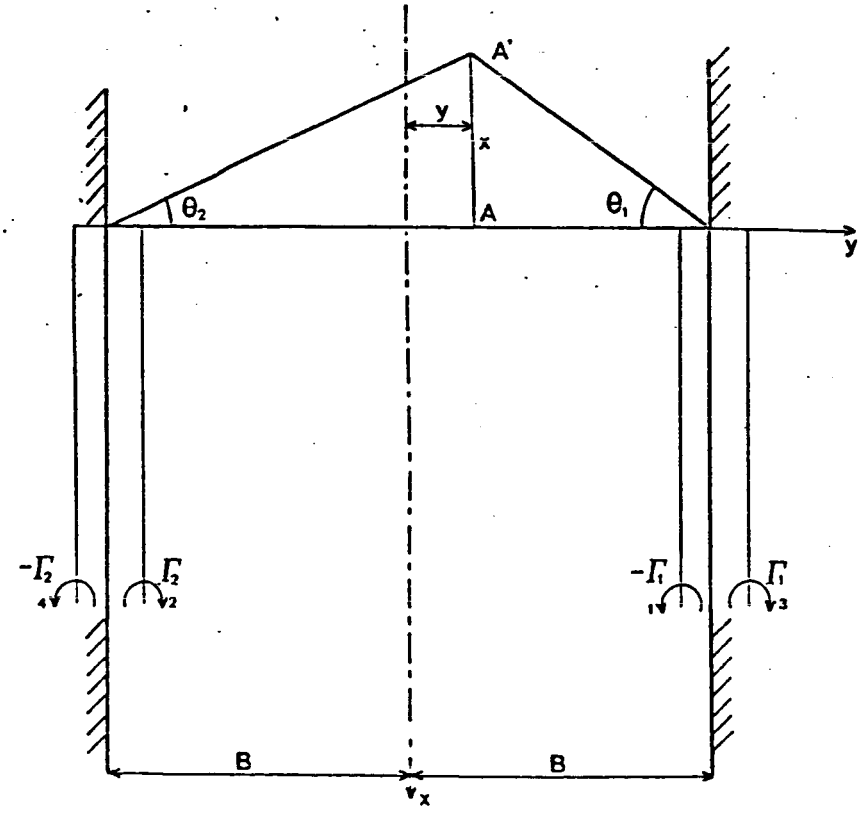

FIGURE 18

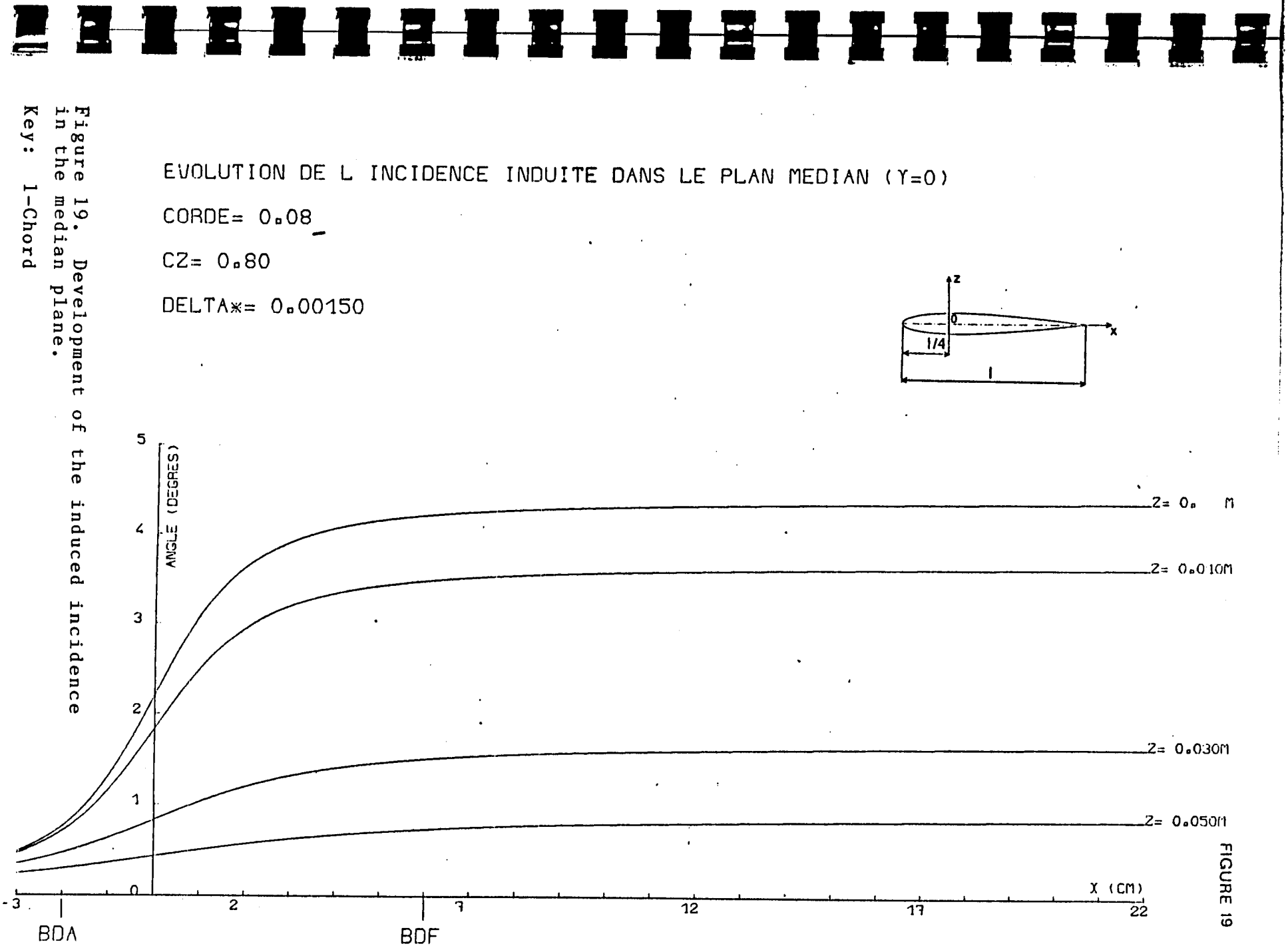

Figure 19. Development of the induced incidence in the median plane.

Key: 1-Chord

FIGURE 19

Figure 20. Development of the induced incidence along the span of the median plane.pf the profile.

Key: 1-Chord.

FIGURE 20

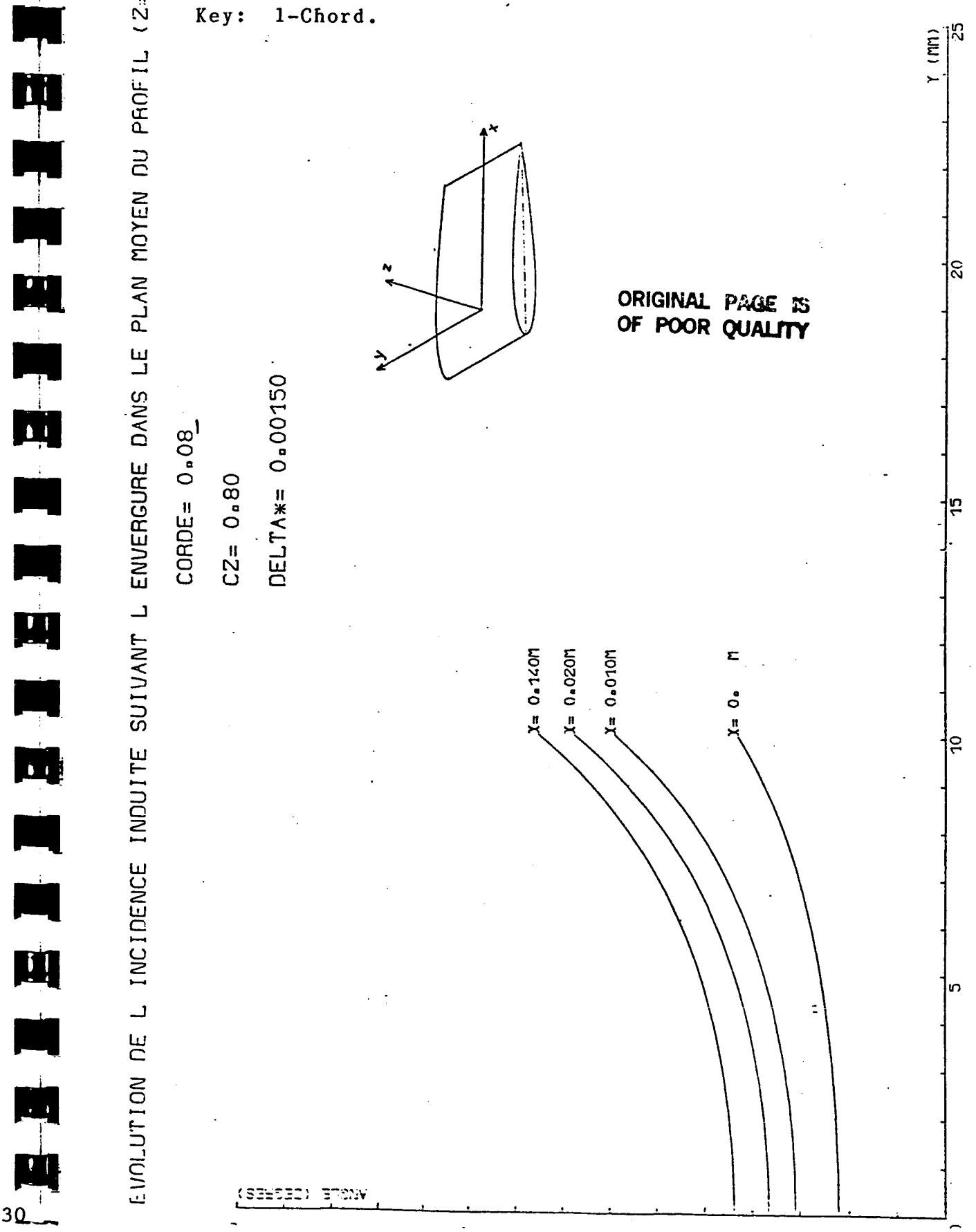

Figure 21. Profile of boundary layer-hologram side.

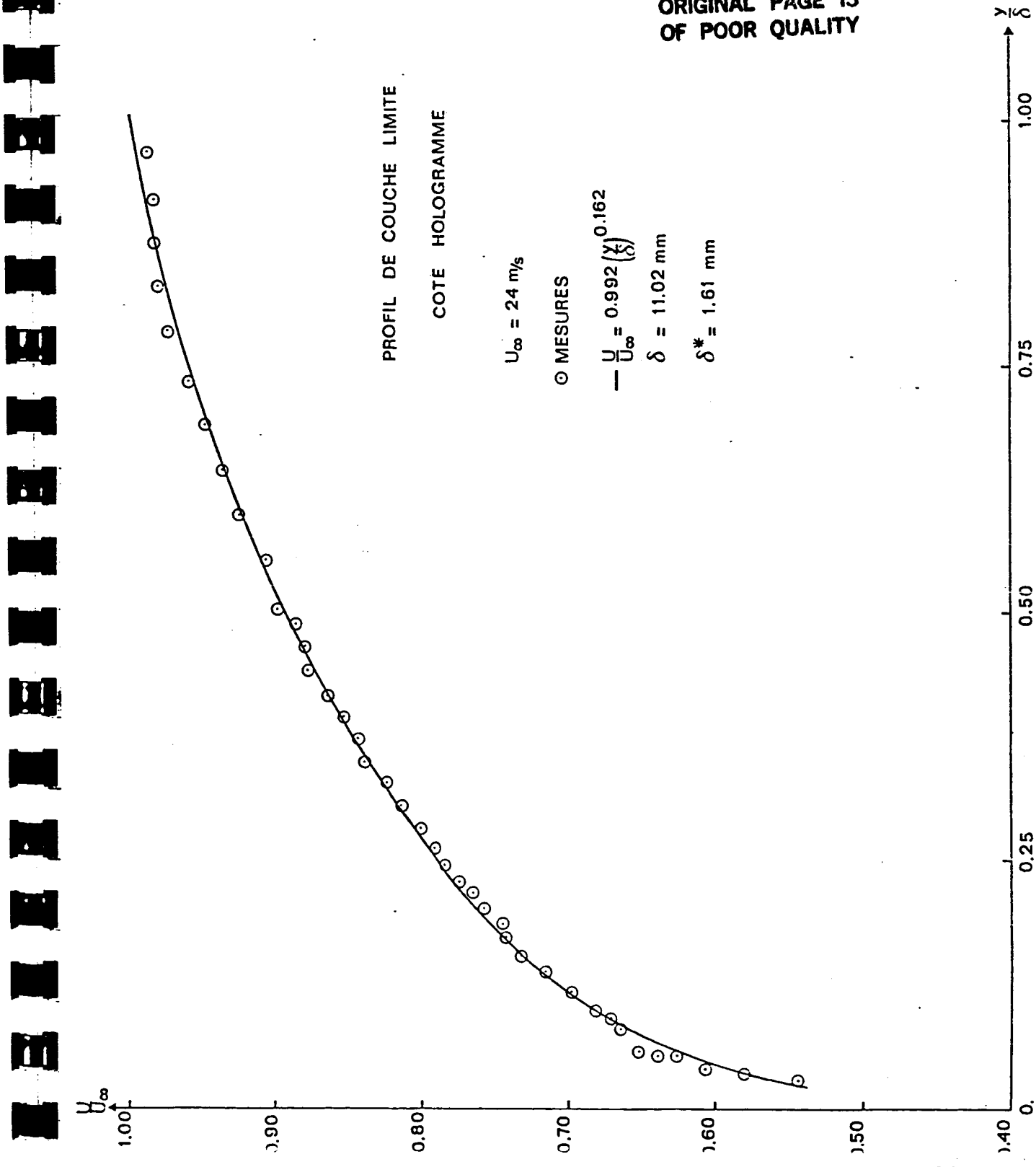

Figure 22. Profile of boundary layer-laser side.

FIGURE 22

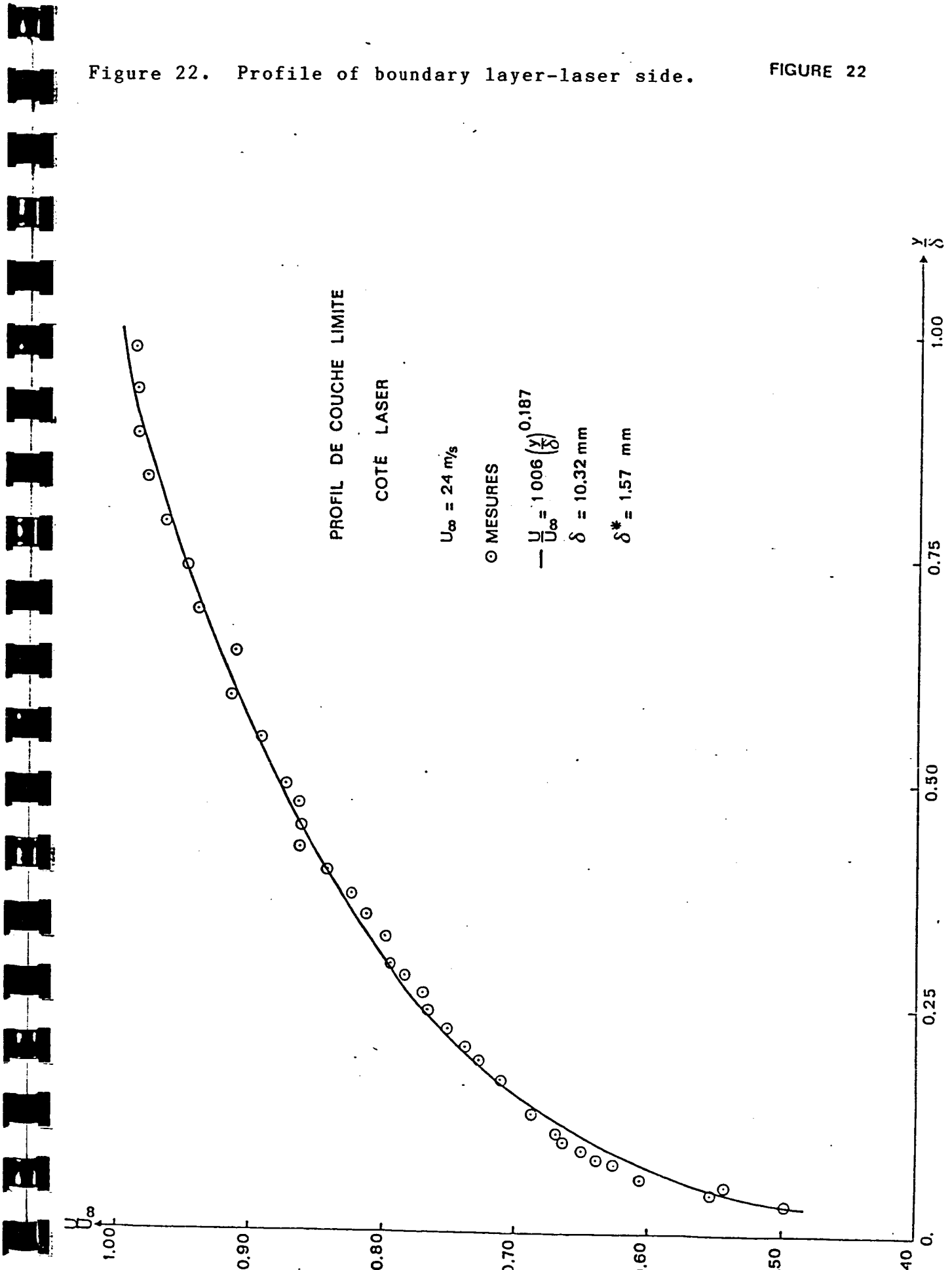

FIGURE 23

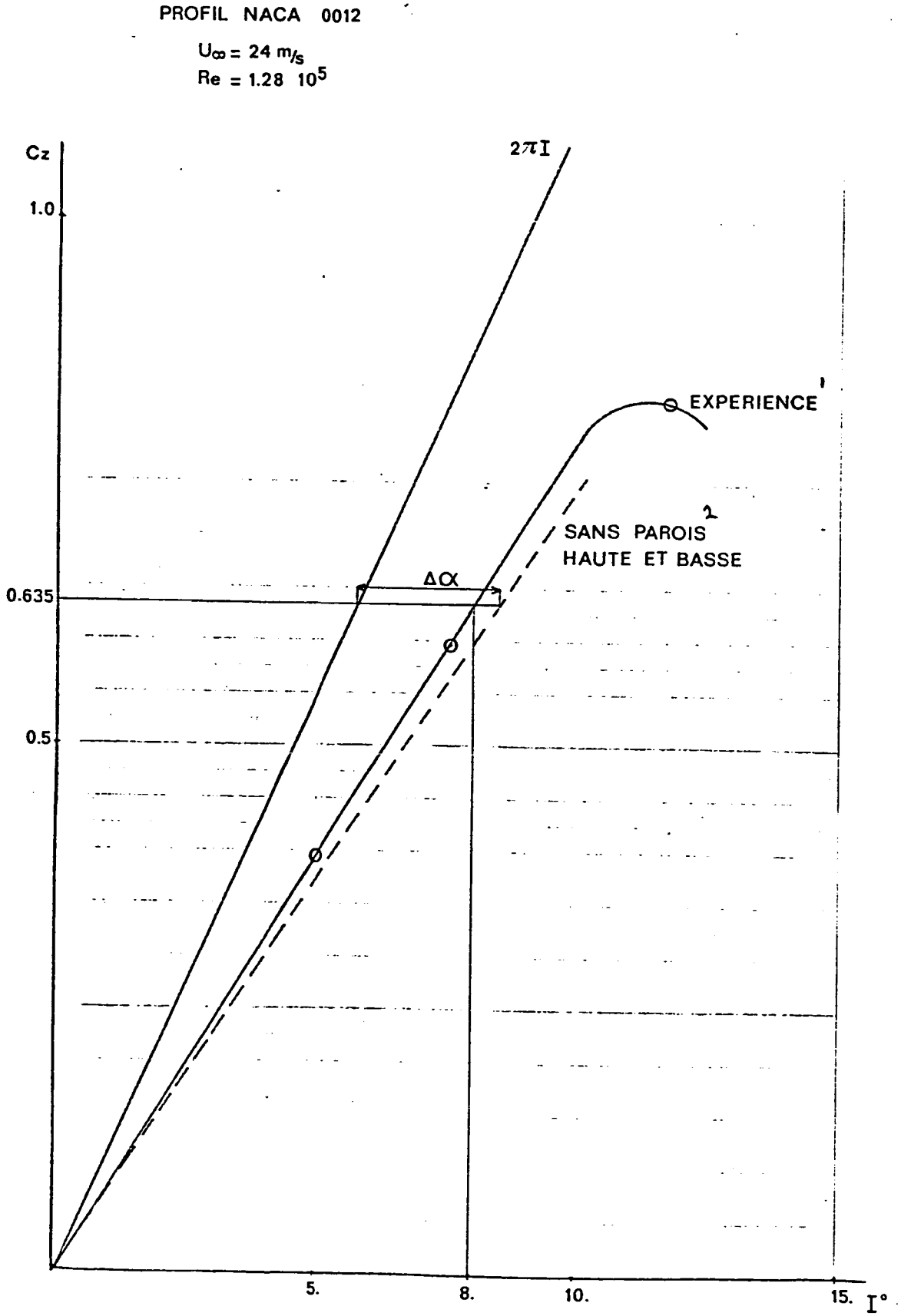

Figure 23. NACA 0012 Profile.

Key: 1-Experimental 2-Without upper and lower walls

ORIGINAL PAGE IS
OF POOR QUALITY

FIGURE 24

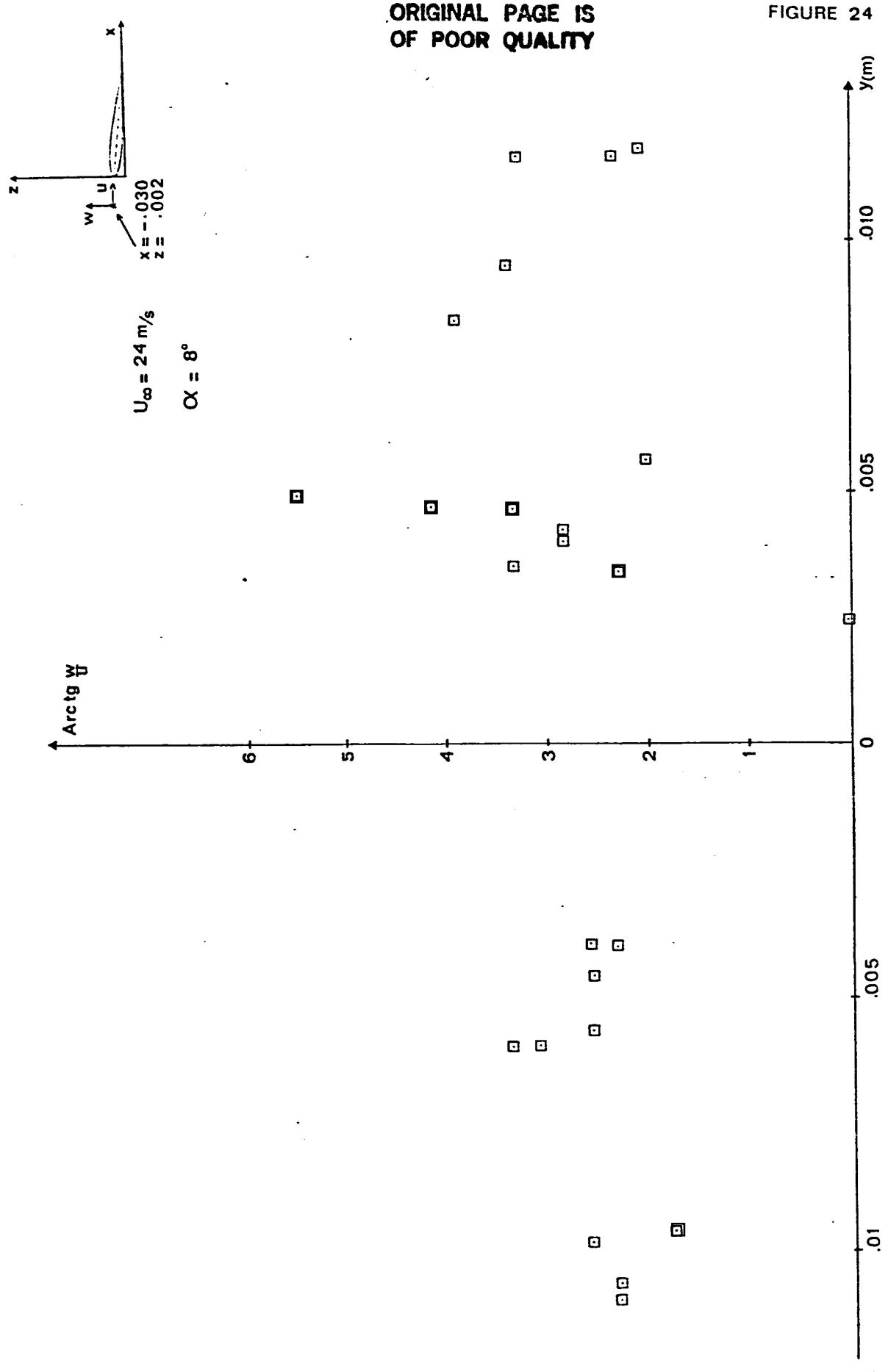

FIGURE 25

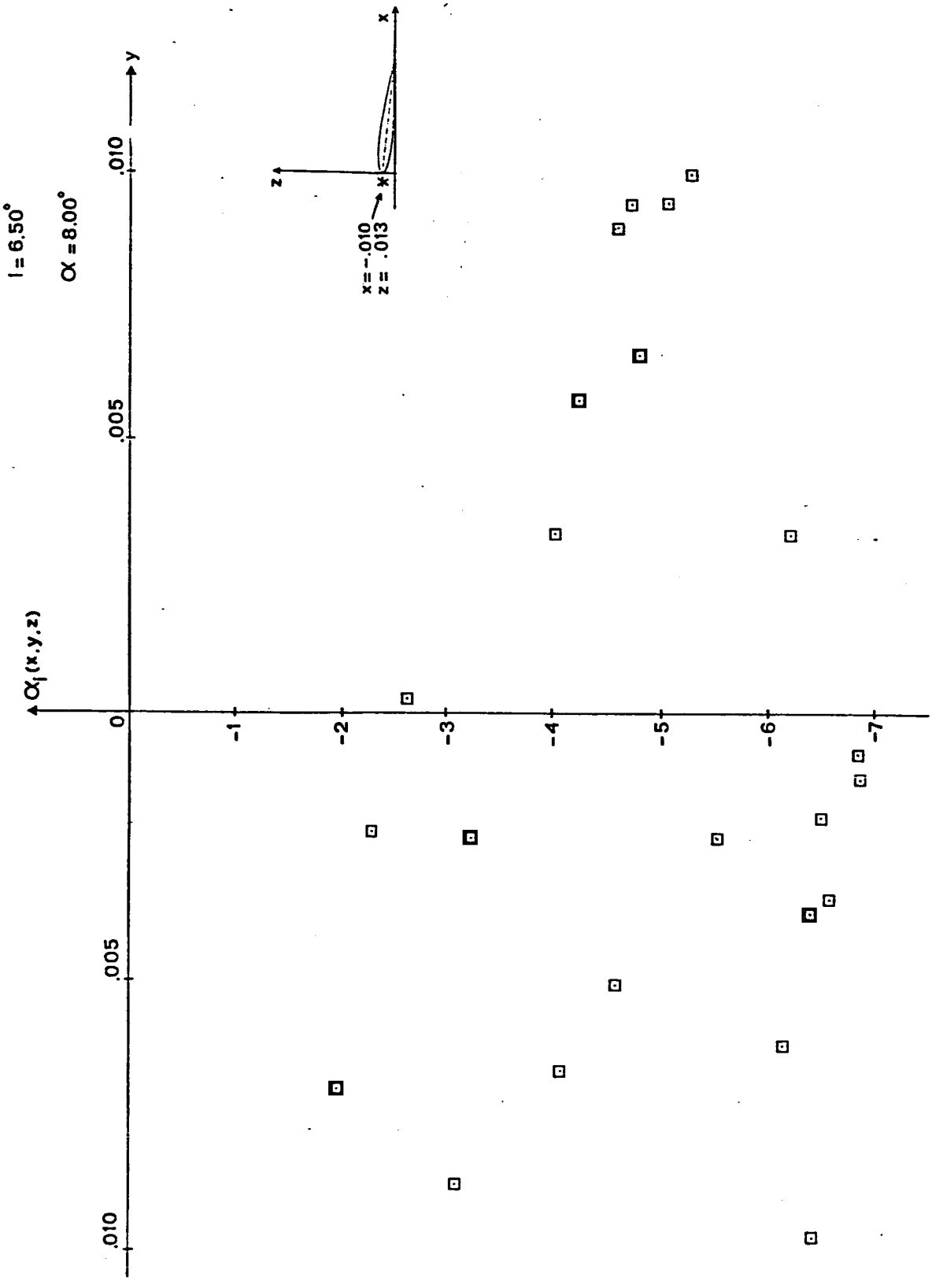

STANDARD TITLE PAGE

1. Report No. NASA TM-88486	2. Government Accession No.	3. Recipient's Catalog No.
4. Title and Subtitle STUDY BY DOUBLE EXPOSURE HOLOGRAPHY OF THE THREE-DIMENSIONAL CHARACTER OF THE FLOW AROUND AN AIRFOIL PROFILE IN A WIND TUNNEL		5. Report Date September 1986 6. Performing Organization Code
7. Author(s) G. Heid and M. Stansilas		8. Performing Organization Report No. 10. Work Unit No.
9. Performing Organization Name and Address Leo Kanner Associates Redwood City, California 94063		11. Contract or Grant No. NASw-[redacted] 4005 13. Type of Report and Period Covered Translation
12. Sponsoring Agency Name and Address National Aeronautics and Space Administration, Washington, D.C. 20546		14. Sponsoring Agency Code

15. Supplementary Notes

Translation of "Etude par holographi à double exposition du caractere tridimensionnel de l'écoulement autour d'un profil d'aile en soufflerie", Institut de Mécanique des Fluides de Lille, Lille, France, Report No. 80/31, July 3, 1980, pp. 1-34 (82N22474).

16. Abstract

17. Key Words (Selected by Author(s))	18. Distribution Statement Unlimited-Unclassified		
19. Security Classif. (of this report) Unclassified	20. Security Classif. (of this page) Unclassified	21. No. of Pages	22.